

# Design and Analysis of a Multi-Port Microgrid to DC Bus Control for a Robotic System

Vinicius de Oliveira Coelho, Anderson José Balbino,  
Lucas Raphael de Jesus da Silva

Department of Electrical and Electronic Engineering  
Federal University of Santa Catarina  
Florianópolis-SC, Brazil  
viniciusoliveira2703@hotmail.com,  
andersonjbalbino@gmail.com, lucasrph2000@gmail.com

Guilherme Batista  
Department of Automation and Systems  
Federal University of Santa Catarina  
Florianópolis-SC, Brazil  
guilhermebatista111@gmail.com

Vinicius Noal Artmann, Henrique Simas, Daniel  
Martins

Department of Mechanical Engineering  
Federal University of Santa Catarina  
Florianópolis-SC, Brazil  
vinicius.artmann@gmail.com, henrique.simas@ufsc.br,  
danielmc@gmail.com

Roberto Kinceler  
Celesc Distribuição S.A.  
Florianópolis-SC, Brazil  
rkinceler@celesc.com.br

**Abstract**— This paper focuses on analyzing and designing the control system in a DC microgrid, which is responsible to provide energy for a robotic system built to inspect distribution power lines. The microgrid was projected to feed sensors, microcontrollers, and a DC motor. Also, in order to provide energy for the system, lithium-ion batteries and photovoltaic cells are employed as sources of the microgrid. With this architecture, the control system is designed to adjust the current/voltage references, to ensure the power balance in the DC microgrid. To corroborate the proposed structure, simulation results are presented under different scenarios of irradiance, temperature, load steps, and torque oscillations in the DC motor.

**Keywords**— *Robotic system, DC microgrid, energy storage system, photovoltaic energy.*

## I. INTRODUCTION

The electrical power system is a complex set of different components that must operate with precision to provide electrical energy to consumers. Although, making everything work harmoniously for a long period of time becomes a great challenge, due to the amount of items that make part of the system, and, hence, must be analyzed, avoiding that people be harmed due to problems that can occur in the process, as faults in the distribution lines. Another feature that also brings a significant challenge is due to the non-linear characteristics of the electrical lines and unforeseeable disturbances, what makes the search for a defect and its isolation expensive for the companies, and requires a lot of time to be done [1].

Hence, the built of artificial intelligences, able to monitor, detect and classify different types of faults have been the object of study in the past 20 years [2]. One of the solutions found is the employment of a neural network in a robotic system, that should be positioned in the lines to perform an inspection in its elements, searching for possible failures in insulators, fuses, and cables, as defects on their structure, or

excessive increases in the superficial temperature, warning to the company about it, enabling this one to do a rapid repair.

In order to build a robotic system as the one described before, a dc microgrid is required, which is the object of study in this paper. This is a solution for power distribution applications that modular expansion, efficiency, and integration of renewable energies are required [3]. To this purpose, a lithium-ion batteries bank, that performs the battery energy storage system (BESS), and photovoltaic cells are being used as sources in this project. To integrate various energy sources in a microgrid, a multiport converter for connecting multiple sources or an individual converter for each source can be used [4]. The structure selected in this project was that each component is coupled on the system by a converter, and will be employed to provide energy to the following loads: visual and thermal cameras, microcontrollers, sensors, and a DC motor. Also, a battery pack is used to provide energy to all the loads, while a PV system is added to provide additional energy and, depending on the operation mode, charge the BESS [4]. To guarantee the photovoltaic panels reach their maximum power point, an algorithm is needed (also called MPPT control), but this is not an object of study in this paper.

In order to connect all of the components in a common bus, different dc-dc converters were projected to create a DC bus. They are also responsible for managing the power flow between sources and loads synchronously with a power management algorithm, however, this algorithm will not be explored in this paper.

During the robot operation, changes can occur at any time, such as dynamic variations in torque motors and irradiance steps. To achieve the power flow requirements and guarantee controllability, reliability and stability for the DC microgrid, a control system was proposed [5]. It's objective is to ensure

appropriate time responses to any part of the circuit, overshoots that respects the demands of the loads, and that all of them receive enough power to operate safely.

This paper is structured as follows. The second section describes the system configuration, the components, and its parameters. The third section shows the control system proposed, including the project of the controllers, and the parameters that must be accomplished during the dc microgrid operation. The fourth section discusses the simulation results in software *PSIM*<sup>®</sup>, analyzing the system behavior towards the stability and the power flow between the components. The fifth section is dedicated to showing the conclusions.

The R&D project that made this work possible was entitled “Robotized System for Inspection of Electrical Distribution Lines” (05697-0317/2017), being financed by Centrais Elétricas de Santa Catarina (Celesc), executed by the Raul Guenther Applied Robotics Laboratory, and administered by the Foundation for Education and Engineering of Santa Catarina (FEESC).

## II. SYSTEM OVERVIEW

The circuit structure is shown in Fig. 1. As can be seen, the photovoltaic panels are coupled to the DC bus with a boost converter. The battery bank is interfaced with a bidirectional buck-boost converter, characteristic that allows the storage system providing/receiving energy to/from the rest of the circuit. The microcontrollers and sensors are connected in the system by buck converters. As the DC motor needs a half-bridge to drive and control, two converters in series were used. The first one, connected directly in the dc bus, is a boost converter, used to energize the half-bridge, while the second is a buck converter and feeds the DC motor.

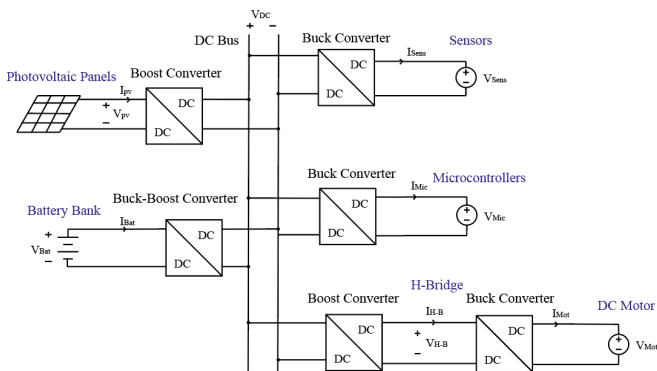


Fig. 1. Grid configuration and the proposed control system

## III. CONTROL STRATEGY AND STABILITY ANALYSIS

The DC microgrid requires control to keep the system stable under any operation and to balance the power between loads and sources. For this purpose, a decentralized control strategy is used to reach such objectives, whose reference values are provided by the power management algorithm cited in section I.

The reason for choosing this strategy is characterized is the fact that a digital communication link is unnecessary,

This work was developed under the Electric Energy Sector Research and Technological Development Program regulated by ANEEL

increasing reliability and reducing costs [6]-[7]. The system parameters are described in Table I.

The controllers used in this paper are the proportional-integrals (PI), due to its characteristic of providing null error in steady-state, while improving the gain in low frequencies [6]. The project methodology requires from the controllers, that each converter have a phase margin,  $MF_{Req}$ , between  $45^\circ$  em  $90^\circ$ , and a gain margin of 6dB, at least [8]-[9]. The stability analysis will be dedicated only for the DC bus control strategy, as will be seen in the next section

### A. Proposed Control Scheme for BESS

Figure 2 presents the control system proposed for the bidirectional buck-boost converter, composed of an external output voltage control loop and an internal inductor current control loop.

The first loop will be applied to control the DC bus voltage  $V_{DC}$ , while the second will manage the charging and discharging of the batteries [10]. Hence, with the measured  $V_{DC}$ , the  $G_{vDC}$  (s) controller will adjust this voltage value, providing a reference to the inductor current  $i_{L,Bat}$ . After this, the  $G_{iBat}$  (s) controller will send the duty cycle reference to a PWM signal generator, in order to drive the converter switches.

TABLE I – System parameters

DC Microgrid Parameters	
DC Bus ( $V_{DC}$ )	18 V
Battery Voltage ( $V_{Bat}$ )	12 V
Sensors Voltage ( $V_{Sens}$ )	3.3 V
Microc. Voltage ( $V_{Mic}$ )	5 V
Half-Bridge Voltage ( $V_{H-B}$ )	32 V
Motor Voltage ( $V_{Mot}$ )	24 V
PV Modules Voltage ( $V_{PV}$ )	15 V
Switching Frequency ( $f_s$ )	50 kHz

In the controllers project, to ensure that both loops operate without interfering with each other, the dynamic decoupling must be respected. To achieve this, the cutoff frequency of the voltage loop  $f_{V_{Bat}}$  must be, at maximum, a decade lower than the switching frequency  $f_s$ . Also, the cutoff frequency of the current loop  $f_{i_{Bat}}$  must be, at least, a decade lower than  $f_{V_{Bat}}$  [11]-[12].

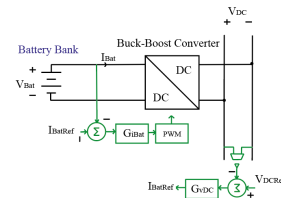


Fig. 2. Control scheme of the buck-boost converter

### B. DC Bus Stability Analysis

To analyze the DC bus stability, firstly it is necessary to obtain the transfer functions of the uncompensated system. The internal loop transfer function and inductor current controller are given respectively by:

$$G_{idBat}(s) = \frac{i_L(s)}{d(s)} = \frac{V_{DC}}{L_{Bat}s} \quad (1)$$

$$C_{ibBat}(s) = K_{idBat} \frac{(1+T_{idBat}s)}{T_{idBat}s} \quad (2)$$

where  $L_{bat} = 1.44$  mH,  $K_{idBat} = 0.75$ , while the zero is positioned in  $1/T_{idBat} = 6.25$  rad/s. Hence, the open loop transfer function, that relates the output voltage to the reference voltage is:

$$FTMA_{vBat}(s) = G_{viBat} \frac{G_{idBat} \cdot C_{idBat}}{1+G_{idBat} \cdot C_{idBat}} \quad (3)$$

where

$$G_{viBat}(s) = \frac{v_{DC}(s)}{i_L(s)} = \frac{1-D}{V_{Bat}} \cdot \frac{-R_{Bat} \cdot V_{Bat} + L_{Bat} V_{DC}^2 s}{C_{Bat} R_{Bat} s + 1 + D} \quad (4)$$

$V_{Bat} = 12$  V,  $C_{Bat} = 2.5$   $\mu$ F and  $R_{Bat} = 2$   $\Omega$ . With these values, the uncompensated loop has a Bode diagram as shown in Fig. 3(a). Analyzing the graphic, it is notable that the system is unstable, due to the negative value of gain margin ( $MG_{Uncomp} = -26.5$  dB). The phase margin ( $MF_{Uncomp} = 101.92^\circ$ ) also has disagreements, due to the fact that not being inside that range cited in the beginning of this section,  $45^\circ < MF_{Req} < 90^\circ$ .

A compensator that ensures to this system a margin phase inside the required limits and with acceptable value of margin gain is:

$$C_{DC}(s) = K \frac{1+s \cdot T_{DC}(s)}{s \cdot T_{DC}(s)} \quad (5)$$

where  $K = 0.02$  and  $1/T_{DC} = 3.33$  krad/s. The bode diagram of the compensated system is shown in Fig. 3(b). It can be seen that the  $C_{DC}(s)$  allows the DC Bus to operate with stability, ensuring a margin phase and margin gain of  $MF_{Comp} = 81.37^\circ$  and  $MG_{Comp} = 7.47$  dB, respectively.

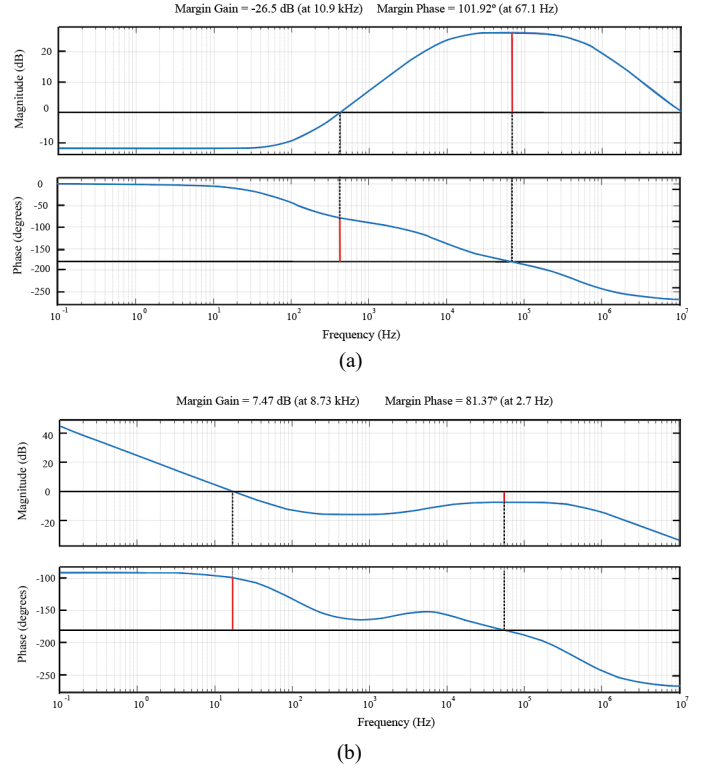


Fig. 3. Bode diagram of DC bus transfer function. (a) Uncompensated system. (b) Compensated system.

### C. Proposed Control Scheme for Photovoltaic Modules

The diagram of the MPPT control for the PV modules is shown in Fig. 4. In this scheme, with the values of photovoltaic voltage and current,  $V_{PV}$  and  $I_{PV}$ , a MPPT algorithm is responsible for finding a reference  $I_{PVRef}$  sent to the current controller  $G_{IPV}(s)$ , which regulates  $I_{PV}$  according to the maximum power point obtained [4].

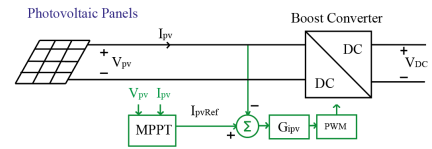


Fig. 4. Control scheme of the photovoltaic cells converter

### D. Proposed Control Scheme for Microcontrollers and Sensors

To control the buck converters that are used to interface the microcontrollers and sensors in the microgrid, a simple voltage control loop is required, as can be seen on Fig. 5. Just like the case of the BESS, not just the phase and gain margins are relevant parameters but the cutoff frequency too. For this case, the cutoff frequency of the voltage loop must be, at maximum, a decade lower than  $f_s$ .

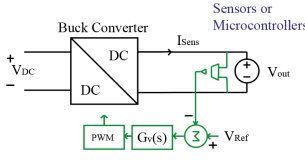


Fig. 5. Control scheme of the buck-boost converter

### E. Proposed Control Scheme for the DC Motor and the Half-Bridge

The proposed scheme is shown in Fig. 6. From the DC bus, a boost converter will increase its value to a higher voltage level, in a way that its output  $V_{H-B}$  will supply the half-bridge. The converter destined to couple the dc motor is in series with the boost. In this case, a buck topology is responsible to decrease the voltage level to a desired value [13], which must match with the field voltage.

In both converters, a double loop control is proposed, thus, the same strategy and principles, as the required margins and the dynamic decoupling that were cited in section III.a, will be repeated here.

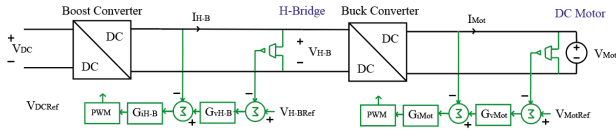


Fig. 6. Proposed control strategy to the half-bridge and the dc motor

## IV. SIMULATION RESULTS AND DISCUSSION

The proposed system is simulated in *PSIM*<sup>®</sup> software, with a time simulation of 4.5 s to test all the possible variations that can occur during the robot operation. The simulation considers a case where the BESS is composed of 4 batteries, each one with a capacity of 3.3 Ah and 100% charged. The performance of the DC microgrid is shown on Figs. 7(a)–(i), while results are discussed in the sequence. All the loads are modeled as variable resistances, which initial values adjusted for the microcontrollers, sensors, dc motor and half-bridge loads are  $R_{Mic} = 5 \Omega$ ,  $R_{Sens} = 2 \Omega$ ,  $R_{Mot} = 96 \Omega$ ,  $R_{H-B} = 160 \Omega$ , respectively.

### A. Case 1: Initialization ( $0 < t < 0.5$ s)

During  $0 < t < 0.5$  s, the system is initialized. The DC bus is maintained at a constant value of 18V, as can be seen on Fig. 7(a). The same result was obtained for waveforms in Fig. 7(b)–(h), that achieved their steady-state values with null error, low overshoots and quick transients (dozens of milliseconds). The solar irradiation and the temperature are  $1000 \text{ W/m}^2$  and  $25 \text{ }^\circ\text{C}$ , respectively, which ensure the photovoltaic modules provide 27 W to the system (Fig. 7(i)). According to Table II, as the loads are demanding a total power,  $P_{Dem}$ , of:

$$P_{Dem} = P_{Mic} + P_{Sens} + P_{Mot} + P_{H-B} = 22W \quad (6)$$

where  $P_{Mic}$ ,  $P_{Sens}$ ,  $P_{Mot}$ , and  $P_{H-B}$  are powers on the microcontrollers, sensors, DC motor and half-bridge, respectively, therefore, the power supplied by the battery bank is:

$$P_{Dem} = P_{PV} \pm P_{Bat} \quad (7)$$

which implies in  $P_{Bat} = -5 \text{ W}$  (according to the notation adopted in this paper, the positive signal indicates energy receiving), hence, in this period of time, the BESS is being charged. This negative value is due to the fact that the dc motor is demanding a low torque, or, equivalently, a low power, that can be supplied by the photovoltaic cells.

TABLE II – Variations on the DC microgrid

System Parameters					
Time (s)	Irradiation	Temperature	Microc. Demand	Sensors Demand	DC Motor Demand
0 – 0.5	1000 W/m <sup>2</sup>	25 °C	5 W	5 W	6 W
0.5 – 1	900 W/m <sup>2</sup>	25 °C	5 W	5 W	6 W
1 – 1.5	900 W/m <sup>2</sup>	28 °C	5 W	5 W	6 W
1.5 – 2	900 W/m <sup>2</sup>	28 °C	10 W	5 W	6 W
2 – 2.5	900 W/m <sup>2</sup>	28 °C	10 W	10 W	6 W
2.5 – 3	900 W/m <sup>2</sup>	28 °C	10 W	10 W	12 W
3 – 3.5	900 W/m <sup>2</sup>	28 °C	10 W	10 W	24 W
3.5 – 4	900 W/m <sup>2</sup>	28 °C	10 W	10 W	48 W
4 – 4.5	900 W/m <sup>2</sup>	28 °C	10 W	10 W	96 W

### B. Solar Irradiations ( $0.5 < t < 1$ s)

The first climate change emulated is on solar irradiation. When  $0.5 < t < 1$  s, it was considered a reduction of  $1000 \text{ W/m}^2$  to  $900 \text{ W/m}^2$ . As was cited on section II.B, this causes a reduction on the maximum power point to 25.2 W, which can be seen in Fig. 7(i), and on the photovoltaic current (Fig. 7(b)), although the photovoltaic voltage maintains in 14.8 V (Fig. 7(h)). However, the MPPT method can ensure that the modules operate in a power near to the maximum. To maintain a power stability, it is necessary a higher power by the batteries (4.8 W, more specifically), which increases the batteries current (Fig. 7(d)). Analyzing Fig. 7, it is interesting to note that the voltage slightly changes during the variation, which implies in an important feature of the control strategy, its capacity to have low sensibility towards this change. The DC bus is successfully maintained on 18V throughout this period of time.

### C. Temperature Changes ( $1 < t < 1.5$ s)

The second climate change was an increase in the temperature of  $25 \text{ }^\circ\text{C}$  to  $28 \text{ }^\circ\text{C}$ , during  $1 < t < 1.5$  s. This causes another reduction on the MPPT to 23.2W, which again implies an increase on the batteries power ( $P_{Bat} = -1.2 \text{ W}$ , according (7)) and current. The same characteristic of sensibility, cited on

section IV.B can be seen here. Again, the system does not suffer with fluctuations during this variation.

#### D. Microcontrollers and Sensors (1.5 < t < 2.5 s)

For t = 1.5 s, it was simulated that the microcontrollers need twice power, in relationship to the one required before. Another variation considered was on the sensor's demand, in t=2s, where, as the microcontrollers case, will also need twice power. In terms of simulation, this situation can be modeled as a reduction on the equivalent resistances, in a way that, with these changes,  $R_{Mic} = 2.5 \Omega$  and  $R_{Sens} = 1 \Omega$ . Hence, in the final of this period of time, the loads will require from the sources a total power of  $P_{Dem} = 32 \text{ W}$ . As the PV modules cannot provide enough energy to the system, the battery bank discharges in order to supply part of it.

In comparison to the other variations, in this two cases, it is noted that the system detects it, but the control strategy can suit this situation, in order to ensure that the waveforms only have low variations on the overshoots and quick responses, as can be seen during 1.5 < t < 2.5 s. Again, the voltage levels are reached after the transients, while the DC bus is maintained at one 18 V.

#### E. DC Motor and Half-Bridge (2.5 < t < 4.5 s)

Now, the robotic system is starting to accelerate, what requires from the dc motor a higher torque according to the time, what, can be expressed, on the simulations, as decreases on the equivalent resistances. During each variation, it is considered that the dc motor will need twice power.

Firstly, at t = 2.5 s, the dc motor will require  $P_{Mot} = 12\text{W}$  (twice, in comparison to power requisite before) from the dc microgrid, which also provokes, from the half-bridge, a demand of  $P_{H-B}=12\text{W}$ , what results in  $R_{Mot} = 48 \Omega$ . The second load step occurs on t = 3 s, in a way that  $P_{Mot} = 24\text{W}$ , hence  $R_{Mot} = 24 \Omega$ . The third step occurs in t = 3.5 s, therefore  $P_{Mot}=48\text{W}$ ,  $R_{Mot} = 12 \Omega$ . Finally, in t = 4 s, the motor arrives in the maximum torque possible,  $P_{Mot} = 96\text{W}$ , implying in  $R_{Mot} = 6 \Omega$ . The period of 4 < t < 4.5 s is the one where the system is operating on its maximum power, that is, according (7),  $P_{Max} = 115 \text{ W}$ .

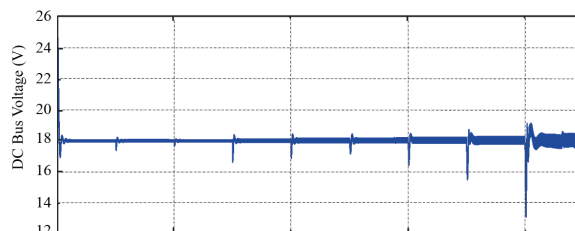
Analyzing this time interval, it can be seen by Fig. 7(f)-(g), that the variations do not provoke much effect on the microcontrollers and sensor converters, allowing them to operate properly. The principal change is on the half-bridge, DC motor and DC bus voltage waveforms.

Firstly, its overshoots get higher according to the load steps. In practice terms, this can be understood as the inertia action on the system, because, according to the motor requires more power, current and voltage peaks are needed. The second feature that must be appointed is that the time responses stay lower. However, it is not a problem for the simulation, once electrical machines take some time to drive until they arrive in the needed torque, therefore the time responses obtained are as expected.

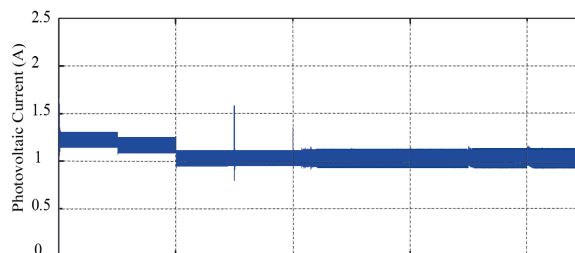
During this time interval, the battery current also has some differences. The principal one is that higher power steps cause

higher values on its steady-state. The most notable example is when 3 < t < 4 s. Seeing the Fig. 7(i), the current passes from 6.75 A to 14.3 A, indicating an increase of 111.9%, approximately.

Another important characteristic, which can be seen on Fig. 7(a),(c)-(d) is the increase in the voltage ripples. This is due the fact that the values of capacitances and inductances on the converters depend on the load resistance, input and output voltages, duty cycle, capacitor voltage and inductor current ripples, and the switching frequency. Hence, from the moment that the powers in the dc motor and half-bridge increase, the only parameter that can be changed, in order to balance the energy flow through the system, is the ripple, which is inversely proportional to the resistance loads. A viable solution for this case is to increase the value of the bus capacitance, however this approach will not be the object of study in this paper.



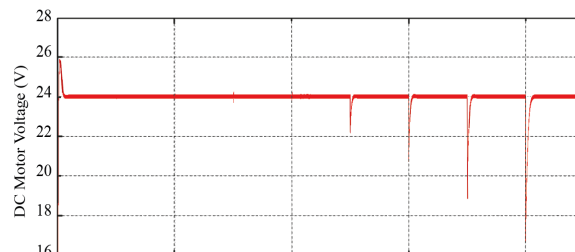
(a)



(b)



(c)



(d)

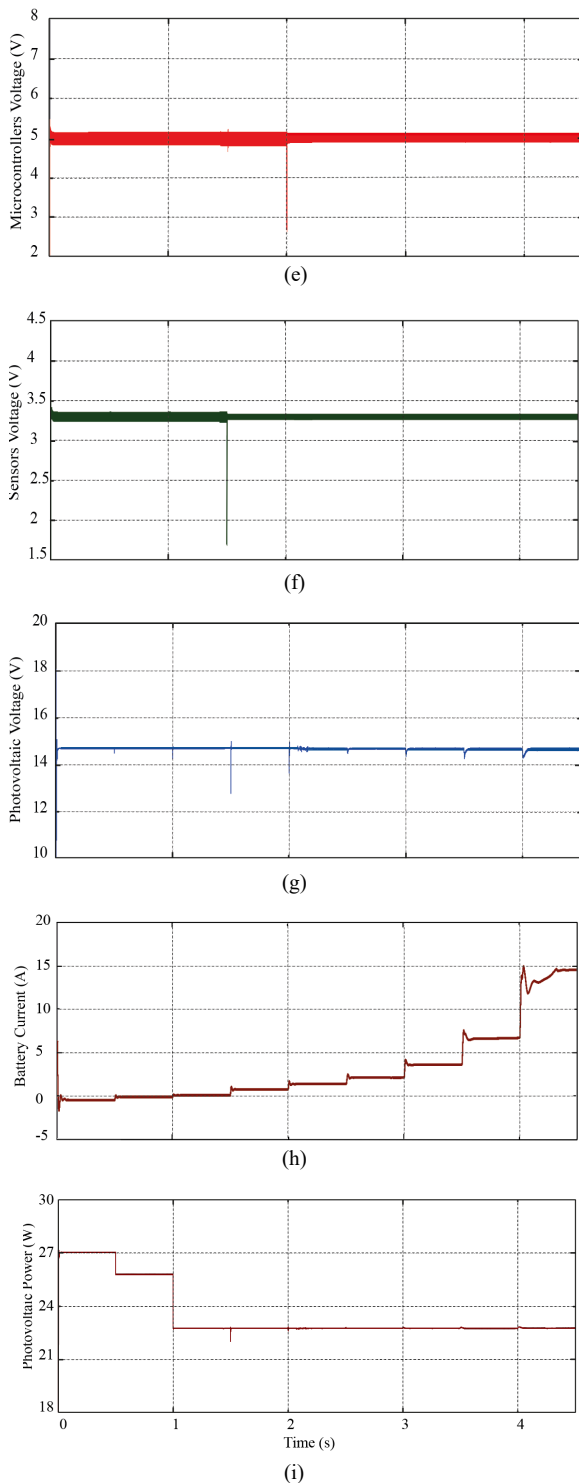


Fig. 7. Simulation results of the proposed dc microgrid. (a) DC bus voltage. (b) Photovoltaic cells current. (c) Half-bridge voltage. (d) DC motor voltage. (e) Microcontrollers voltage. (f) Sensors voltage. (g) Photovoltaic cells voltage. (h) Battery current. (i) Photovoltaic modules power.

## V. CONCLUSION

This paper proposed a decentralized control strategy developed for management of power flow in a multiport DC microgrid, and is destined to energize a robotic system. The simulation results explore different situations that can occur during the robot operation on the distribution line, and that must be considered on the system design. But, as can be seen in section IV, all the waveforms have overshoots that do not exceed voltage and current on each component, and suitable time responses. Hence, with this method, it is ensured by the sources, a stable power supply to all the loads, allowing them to operate properly, maintaining an efficient parallelism and the system reliability. This method also provides a reduction of costs, because the sensing can be done with current sensors and simple voltage dividers, and, at the same time, it is not necessary to use a link communication between the converters. Another feature that contributes to the cost reduction is the use of ion-lithium batteries as energy storage systems, because its characteristics are enough to supply the energetic density that is required [15], principally to the dc motor, in order that it is not necessary supercapacitors in parallel with the batteries.

## REFERENCES

- [1] P. Eboule; J. H. Pretorius; N. Mbuli; C. Leke, "Fault Detection and Location in Power Transmission Lines Using Concurrent Neuro Fuzzy Technique"
- [2] K. Chen; C. Huang; J. He, "Fault Detection, Classification and Location in Transmission Lines and Distribution Systems: a Review on the Methods," *High Volt.*, 2016. vol. 1.
- [3] F. C. Santos, "Controle Coordenado de Conversores CC-CC com Saídas Conectadas em Paralelo Voltado ao Processamento de Energia Solar Fotovoltaica.," *Dissertação (Mestrado) — Universidade Federal de Santa Catarina*, 2017.
- [4] X. Xiong and Y. Yang, "A Photovoltaic-Based DC Microgrid System: Analysis, Design and Experimental Results," *Electronics* 2020, pp. 941-958
- [5] S. Kotra; M. K. Mishra, "A Supervisory Power Management System for a Hybrid Microgrid with HESS", *IEEE Transactions on Industrial Electronics*, vol. 64, no. 5, May 2017
- [6] A. P. N. Tahim, "Controle de Microredes de distribuição de energia elétrica em corrente contínua.," *Dissertação (Mestrado) — Universidade Federal de Santa Catarina*, 2015.
- [7] J. Zeng, W. Qiao, L. Qu, and Y. Jiao, "An Isolated Multiport Bidirectional DC-DC Converter for PV-Battery-DC Microgrid Applications," *IEEE J. Emerging Sel. Topics Power Electron.*, vol. 2, no. 1, Mar. 2014
- [8] K. Ogata, "Engenharia de Controle Moderno," 5a ed., [S.l.]: Pearson, 2011.
- [9] I. Barbi, *Projeto de Fontes Chaveadas*. [S.l.]: Florianópolis, 2007
- [10] S. Kotra, and M. K. Mishra, "Dynamic Energy Management of Renewable Grid Integrated Hybrid Energy Storage System," *IEEE Trans. Ind. Electron.*, vol. 64, no. 5, pp. 3640-3649, May. 2017.
- [11] M. Wenk, "Estudo, Modelagem e Controle de Conversor CC-CC Bidirecional Não-Isolado Baseado na Célula de Comutação de Três Estados.," *Dissertação (Mestrado) — Universidade Estadual de Santa Catarina*, 2019.
- [12] R. W. Erickson.; MAKSIMOVIC, D. *Fundamentals of power electronics*. [S.l.]: Springer, 2001. ISBN 0792372700.
- [13] D.C. Martins; I. Barbi. *Conversores CC-CC Básicos Não-Isolados*, 2.ed.
- [14] W. Elsrogy; M. A. Fkirin; M. A. Hassan. "Speed Control of DC Motor Using PID Controller Based on Artificial Intelligence Techniques," *CoDIT 2013*, December 2015
- [15] T. B Lazzarin. "Estudo e implementação de um carregador de baterias com uma técnica de avaliação de sua vida útil". *Dissertação (Mestrado) — Universidade Federal de Santa Maria*, Março. 2006